American Mineralogist, Volume 89, pages 319–326, 2004

Crystal-chemistry of talc: A near infrared (NIR) spectroscopy study

SABINE PETIT,[1,*] FRANÇOIS MARTIN,[2] ANDRZEJ WIEWIORA,[3] PHILIPPE DE PARSEVAL,[4] AND ALAIN DECARREAU[1]

[1]Université de Poitiers, CNRS UMR 6532 HydrASA, 40, avenue du Recteur Pineau, 86022 Poitiers Cedex, France
[2]Université de Limoges, CNRS UMR 6532 HydrASA, 123 avenue Albert Thomas, 87000 Limoges, France
[3]Institute of Geological Sciences, Polish Academy of Sciences, ul. Twarda 51/55, 00-818 Warszawa, Poland
[4]Equipe Géomarg, UMR 5563 du CNRS, LMTG, 39, allées Jules Guesde, Université Paul Sabatier, 31000 Toulouse, France

ABSTRACT

The crystal-chemistry of fifteen samples of talc from various localities and origins having a relatively wide range of Fe, Al, and F contents, have been studied mainly by Fourier-transform infrared (FTIR) spectroscopy, in both the near infrared (NIR) and middle infrared (MIR) regions, and by Mössbauer spectroscopy. For the first time, assignments have been made for the 2νOH bands in talc, and Mg/Al substitutions were revealed using NIR. Less than 0.01 atom of Fe^{2+} or Al per half unit cell can be detected from the 2νOH region, whereas the sensitivity is about half in the νOH region. The amounts of F also can be quantified by NIR measurement, using the F inductive effect on the width of the $2\nu Mg_3OH$ band. The NIR data show that Fe^{2+} and Mg are distributed randomly in their octahedral sheet. Actual structural formulae of natural talcs can be obtained from NIR and Mössbauer spectroscopies only, even for impure talc samples. NIR spectroscopy is simple to use and is a very powerful tool to study the crystal chemistry of talc.

INTRODUCTION

Talc is used in a large number of industrial applications such as papers, paints, ceramics, cosmetics, and polymers (e.g., Menczel and Varga 1983). For example, the use of talc as a filler in polymers induces modifications in crystallization of the resulting composite, causing an increase of the mechanical properties (e.g., Tiganis et al. 1996; Gonzalez et al. 1995; and Ferrage et al. 2002) and thus an industrial interest of the material. However, various difficulties appear using talc, notably an undesirable coloring in ceramics and polymers (blush), and a variable behavior in polymer applications possibly due to oxidation of structural Fe or to the possible occurrence of negative charges on the talc surface (Martin et al. 1999). The aim of the present work is to provide an easy tool for the analysis of talc for a better industrial use.

To calculate the actual structural formula of talc, the analyzed cations must be distributed correctly over the available structural sites. However, a particular difficulty arises either from the presence of impurities, or of trivalent cations such as Fe^{3+} and Al that occur at both the octahedral and tetrahedral sites.

FTIR spectroscopy is a powerful tool to characterize the octahedral composition of talc (and many other hydroxylated minerals), due to the possibility of recognizing the cationic environment of their OH groups via hydroxyl bonds vibrations. However, FTIR spectroscopy so far has been used mainly in the MIR region (4000–400 cm^{-1}). In addition to the MIR region, where fundamental vibrational modes appear, the NIR region (11000–4000 cm^{-1}) also can be used to determine the crystal chemistry of talc.

The popularity of NIR spectroscopy has increased greatly in recent years due to significant development in FTIR spectrometers. The application of the diffuse reflectance technique (DRIFT) simplifies sample preparation in comparison with traditional solid-sampling techniques. The DRIFT is especially appropriate in the NIR region where, in contrast to the MIR region, no dilution of the sample is necessary and, therefore, the IR analysis can be very fast and non-destructive. Moreover, field spectrometers work exclusively in the NIR (and visible) region.

The present paper reports the use of FTIR spectroscopy, especially in the NIR region, to characterize the crystal chemistry of several talcs from various localities and origins. The results are compared with those obtained by chemical analyses.

MATERIALS AND METHODS

A list of the studied samples, along with their source localities and chemical compositions, are given in Table 1. The purity of samples was checked by X-ray diffraction (XRD) with a Philips X'Pert apparatus, using random and oriented powders. From XRD data, all samples contain only talc except for sample 5, which contains a minor amount of a 7 Å phase in addition. For most samples, only few mg were available. The chemical compositions of samples were determined with a Cameca SX50 electron microprobe (Paul Sabatier University, Toulouse, France). Operating conditions were 15 kV and 10 nA using natural and synthetic standards: F, topaz; Na, albite; Mg, periclase; Al, corundum; Si, wollastonite; Ti, pyrophanite; Fe, hematite; Ni, nickel. The estimated errors (in wt% element) are Si ± 0.36, Mg ± 0.31, Al ± 0.05, and Fe ± 0.16.

Structural formulae, based on 11 O atoms, are given in Table 2. Iron, Al, and F show significant variations (up to 0.8 Fe, 0.34 Al, and 0.29 F atom per half unit cell). Sample 1, which is dark green, also contains minor Ni.

^{57}Fe Mössbauer absorption spectra were recorded in the "Laboratoire de Chimie de Coordination," Toulouse (France) over the ranges ± 14 mm/s and ± 4 mm/s in 512 channels. The Mössbauer spectrometer is composed of a compact detector γ-system for high counting rates and a conventional constant acceleration Mössbauer device (Wisel). A ^{57}Co (in Rh) source with nominal activity of 50 mCi was used. The spectra were obtained at 80 K to benefit by the 2nd-order Doppler effect and recorded on a Cambera multichannel analyzer coupled to a computer. The isomer shift was recorded with respect to α-Fe metal. To obtain a good absorber sample thickness (Rancourt et al. 1993), the sample concentration approximated 200 mg/cm^2. Powders were finely ground under acetone (to minimize possible oxidization of Fe) and placed in a plexiglass sample holder. Lorentzian line shapes

* E-mail: sabine.petit@hydrasa.univ-poitiers.fr

TABLE 1. Chemical analyses as determined by electron microprobe, and origin of the samples used

% Sample*	SiO_2	Al_2O_3	Fe_2O_3	MgO	NiO	CaO	K_2O	Na_2O	TiO_2	F
(1) Antwerp, Sterling Mine, USA, from ultrabasic rocks (Robinson and Chamberlain 1984)										
	58.02	0.21	15.42	21.10	0.34	nd	nd	tr	nd	0.72
(2) Pink Haïcheng, China, from dolostones alteration										
	63.19	nd	tr	32.08	nd	tr	tr	tr	tr	nd
(3) Liaoyong White, China, from dolostones alteration										
	64.01	tr	tr	31.46	nd	tr	tr	tr	nd	0.30
(4) Liaoyong Pink, China, from dolostones alteration										
	63.81	0.45	tr	31.57	nd	tr	tr	tr	tr	0.22
(5) Gabon, from carbonate alteration										
	62.99	0.07	tr	30.85	nd	tr	tr	0.21	nd	1.44
(6) Set 16, Leon, Spain, from dolostones alteration (Galan-Huertos and Rodas 1973)										
	62.19	0.17	0.16	32.37	nd	nd	nd	tr	nd	1.00
(7) Brazil fourty, Brazil, from ultrabasic rocks										
	63.02	tr	2.07	29.71	nd	tr	tr	tr	tr	tr
(8) T111, Trimouns, France, from dolostones alteration (Moine et al. 1989; Martin et al, 1999; Schärer et al. 1999)										
	61.67	0.19	0.68	31.52	nd	tr	nd	nd	nd	0.16
(9) Guangxi n°1, China, from dolostones alteration										
	62.72	tr	0.45	30.77	nd	tr	tr	tr	tr	0.19
(10) Puebla de Lillo, Spain, from dolostones alteration (Galan-Huertos and Rodas 1973; Tornos and Spiro 2000)										
	62.89	tr	0.35	31.05	nd	tr	tr	nd	nd	0.93
(11) Rabenwald, Austria, from magnesite alteration (Moine et al. 1989)										
	62.32	0.24	0.92	30.04	nd	nd	tr	tr	nd	0.25
(12) Turcja, unknown origin										
	62.51	0.44	0.89	30.21	nd	nd	tr	tr	nd	nd
(13) Sierra Nevada, Spain, from dolostones alteration										
	–	–	–	–	–	–	–	–	–	–
(14) Roc Martin, Afghanistan, from high grade metamorphism talcschist (Kulke and Schreyer 1973)										
	56.71	4.31	0.48	28.24	nd	tr	nd	0.91	0.28	0.30
(15) Egypt, from carbonate alteration (Schandl et al. 1999)										
	60.82	0.08	0.35	29.42	nd	tr	tr	tr	nd	0.24

Notes: nd = not detected; tr = trace; – = not measured.
* (1), (2), (9), (10), (11), (12), (14), (15) from A. Wiewiora; (3), (4), (5), (6), (7), (8), (13) UPS Mineralogy and F. Martin collections.

TABLE 2. Structural formulae of talcs as calculated conventionally (11 oxygen O atom equivalents)

	1	2	3	4	5	6	7	8	9	10	11	12	13	14	15
Si	3.99	3.99	4.02	4.00	4.02	3.99	4	3.96	4.02	4.01	4.01	4.00	–	3.79	4.03
Al	0.017	0	0	0.033	0.005	0.020	0	0.014	0	0	0.018	0.033	–	0.34	0.006
Fe	0.80	0	0	0	0	0.009	0.10	0.037	0.021	0.017	0.044	0.043	–	0.024	0.017
Mg	2.17	3.02	2.95	2.96	2.94	2.99	2.84	3.02	2.94	2.95	2.89	2.85	–	2.81	2.91
Ni	0.02	0	0	0	0	0	0	0	0	0	0	0	–	0	0
Ti	0	0	0	0	0	0	0	0	0	0	0	0	–	0.01	0
F	0.16	0	0.06	0.04	0.29	0.2	0	0.05	0.04	0.19	0.05	0	–	0.06	0.05
OH	1.84	2	1.94	1.96	1.71	1.8	2	1.95	1.96	1.81	1.95	2	–	1.94	1.95
% $^{VI}Fe^{2+}$	92	–	–	–	–	60	53	68	85	65	78	57.5	–	60	65
% $^{VI}Fe^{3+}$	7	–	–	–	–	0	14	18	5	20	0	27.5	–	30	15
% $^{IV}Fe^{3+}$	1	–	–	–	–	40	33	14	10	15	22	15	–	10	20

Notes: The iron atomic distribution are from Mössbauer measurements. – = not measured.

were assumed for deconvolutions, based on least-squares fitting procedures. The χ^2 and misfit values were used to measure the goodness of the computer fit. No orientation effects were observed.

A Nicolet 510 FTIR spectrometer was used to record FTIR spectra at 4 cm^{-1} resolution in the 4000–400 cm^{-1} range (MIR region). The spectrometer was continuously purged with dry air during scanning of the transmission spectra. The KBr pellets, 2 cm in diameter, were prepared by mixing 3 mg of sample with 300 mg of KBr and heated overnight at 110 °C to remove absorbed water.

NIR spectra were obtained using a Nicolet Magna 760 FTIR spectrometer and a DRIFT accessory "Collector" from Spectra-Tech. The spectrometer was equipped with a CaF_2 beam splitter and a PbSe detector. Powdered samples were analyzed without any dilution in a KBr matrix. For each sample, 128 scans were recorded in the 11000–4000 cm^{-1} spectral range with a resolution of 4 cm^{-1}.

Spectral manipulations were performed using the OMNIC software package (Nicolet Instruments Corp.). Band component analysis of the region of interest was carried out using the least-squares peak-fitting program Peak Solve with the Gauss-Lorentz form of each component. The absorption bands for a condensed phase are of Lorentz form, on which secondary factors of both physical (e.g., sample heterogeneity due to chemical variation, grain boundaries, dislocations, and other defects) and instrumental origin impose a Gaussian perturbation. Therefore, a mixed Gauss-Lorentz function was used to adequately model the experimental data (Hawthorne and Waychunas 1988). An example of spectral decomposition is given on Figure 1. The linearity of the residual line was a good indicator of the goodness of the fit.

The bands present in the NIR region are mainly attributed to the first overtone (2ν) and combinations (ν + δ) vibrations of the OH groups (Petit et al. 1999; Madejová et al. 2000).

RESULTS AND DISCUSSION

Comparison between MIR and NIR

In trioctahedral phyllosilicates, each hydroxyl group is bonded to three octahedral cations. The hydroxyl stretching (νOH) wavenumber is affected by the nature of these cations. Up to four νOH bands can be distinguished when Mg is partially replaced by another divalent cation, corresponding to the four possible combinations of the two different cations within the three adjacent octahedral sites (e.g., Farmer 1974). Wilkins and Ito (1967) measured νOH wavenumbers corresponding to various OH groupings in synthetic Mg, Ni, Co, Zn, Fe, Mn, and Cu talcs. As indicated in Table 3, it is not possible to distinguish between Fe and Ni occurring simultaneously in a talc structure through νOH measurements. In our case, this is not a problem because only one sample contains Ni, and in small amount

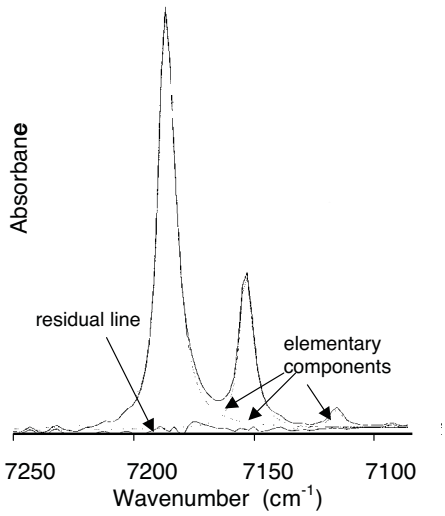

FIGURE 1. Decomposition of the NIR spectra in the 2νOH region of sample 7. The elementary components are in grey. The residual line shows the difference between the fit and the experimental curve.

TABLE 3. Band wavenumbers (±1 cm^{-1}) of the νOH of different groupings of some synthetic talcs reported by Wilkins and Ito (1967)

R	νMg_3OH	νMg_2ROH	νMgR_2OH	νR_3OH
Ni	3677	3663	3646	3625
Fe	3678	3664	3646	3624

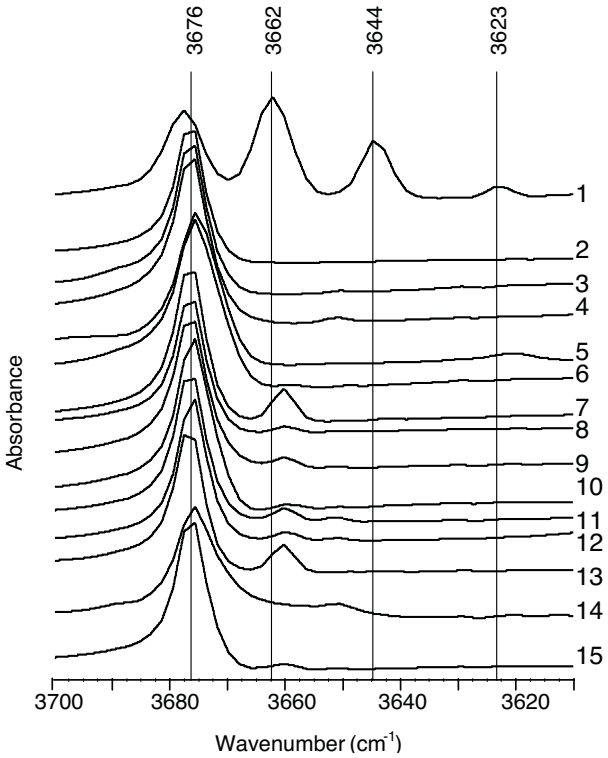

FIGURE 2. FTIR spectra in the νOH region of the talc samples from KBr pellets. Numbers correspond to samples listed in Table 2.

(sample 1, Table 2).

The MIR spectra obtained from natural talcs are in good agreement with the results obtained by Wilkins and Ito (1967) for synthetic talcs. Up to four main bands at about the same wavenumbers as those measured by these authors are observed, depending on the Fe content of the samples (Fig. 2). Following data in Table 3, the bands are logically attributed in this manner: 3676 cm^{-1} / νMg_3OH; 3662 cm^{-1} / νMg_2FeOH; 3644 cm^{-1} / $\nu MgFe_2OH$; and 3623 cm^{-1} / νFe_3OH. The OH-stretching wavenumber of the Mg_3OH group remains almost constant at 3676 cm^{-1}. However, a slight but significant increase of about 2 cm^{-1} of the wavenumber of this band, as well as that of the νMg_2FeOH band, is observed for sample 1, which is Fe-rich compared to the other samples (Fig. 2). These slight changes, which depend on the extent of the substitution for Mg, already have been observed by Wilkins and Ito (1967) for synthetic talcs. Changes in bandwidth are also observed (Fig. 2), and they will be discussed below.

The NIR spectra of the talc samples in the first OH-overtone region (2νOH) (Fig. 3) are similar to those obtained in the MIR region (Fig. 2). The wavenumbers of the overtones are lower than twice the fundamentals because of the anharmonic character of the vibrations (Alpert et al. 1964). By analogy with the MIR region, the 7185, 7156, 7118, and 7073 cm^{-1} bands were assigned to $2\nu Mg_3OH$, $2\nu Mg_2FeOH$, $2\nu MgFe_2OH$, and $2\nu Fe_3OH$, respectively. An additional band at 7136 cm^{-1} is present in some samples and its occurrence is clearly linked to the Al content of the samples. This band is attributed to an OH grouping involving Al, and we tentatively assign it to $2\nu Mg_2AlOH$. By analogy with the NIR, the corresponding fundamental νMg_2AlOH is observed at 3652 cm^{-1} in the MIR (Fig. 2, samples 11 and 14). Such a position corroborates our attribution because, in micas and amphiboles, the wavenumber of the νMg_2AlOH band is at about 20 cm^{-1} less than the wavenumber of the νMg_3OH band (e.g., Robert and Kodama 1988; Robert et al. 2000).

As observed in the MIR, NIR bands are shifted for sample 1, and bandwidth variation occurs: the bandwidth and wavenumber of the $2\nu Mg_3OH$ band of talcs range from 7.1 to 18.5 cm^{-1} and from 7187 to 7183 cm^{-1}, respectively. For sample 1, the small shift of the $2\nu Mg_3OH$ band can be explained by the high Fe content inducing local distortions caused by differences in ionic radii between Mg and Fe^{2+}, as noted previously by Farmer (1974). On the other hand, the $2\nu Mg_3OH$ bandwidth of the studied talcs is correlated with their F contents (Fig. 4). This trend can be explained by an increase in hydrogen bonding between the hydroxyl proton and an O atom linked to Si, and/or by a change in charge distribution within the octahedral sheet due to the different electron withdrawing strengths of F and OH (Rywak and Burtlitch 1996). However, sample 14, and sample 4 to a lesser extent, are off of that trend. Sample 14 is particularly rich in Al. The occurrence of a trivalent cation such as Al, and thus of heterovalent substitutions, generates disorder that can account for band broadening. As a matter of fact, the combination of the inductive effect of F and the Al effect, accounts reasonably well to the broadening of the $2\nu Mg_3OH$ absorption band (Fig. 4): a relatively good correlation is obtained between the number of

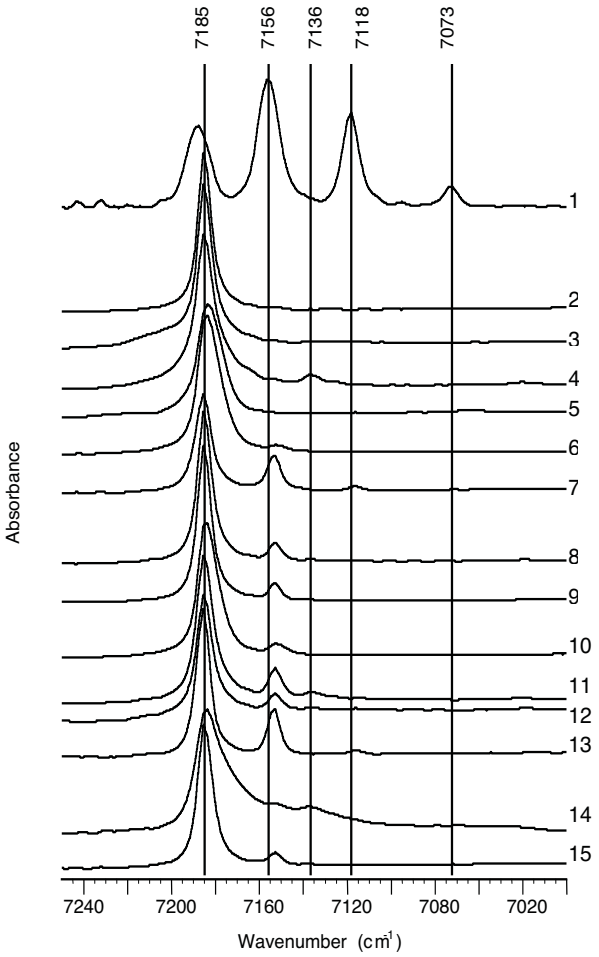

FIGURE 3. FTIR spectra in the first OH overtone region of the talc samples. Numbers correspond to samples listed in Table 2.

(Al + F) atoms per half unit cell and the width of the $2\nu Mg_3OH$ band. The minimum width of the $2\nu Mg_3OH$ band for talc (at room temperature) can also be determined at 6.6 cm^{-1} by extrapolation of the regression line.

Comparing the νOH and 2νOH regions, one can also observe that bands with low intensity in the MIR region are clearly enhanced or even revealed in the NIR region (Figs. 2 and 3). The relative intensities (I) of corresponding absorption bands in both the MIR (νOH) and the NIR (2νOH) regions are compared in Figure 5a. The data from both regions are in good agreement. However, it appears that the Mg_3OH groupings are slightly overestimated (and then the Mg_2FeOH groupings underestimated) in the MIR compared to the NIR.

Chemical composition calculation

The NIR spectra were decomposed as shown in Figure 1 into single-component bands to measure their relative integrated intensities (S). Figure 5b shows that the I and S data for the same bands are in good agreement. However, some departures from the theoretical 1:1 line are observed. The greatest departures from this line (samples 5 and 14) are in the sense of overestimating the abundance of Mg_3OH groupings by direct intensity measure-

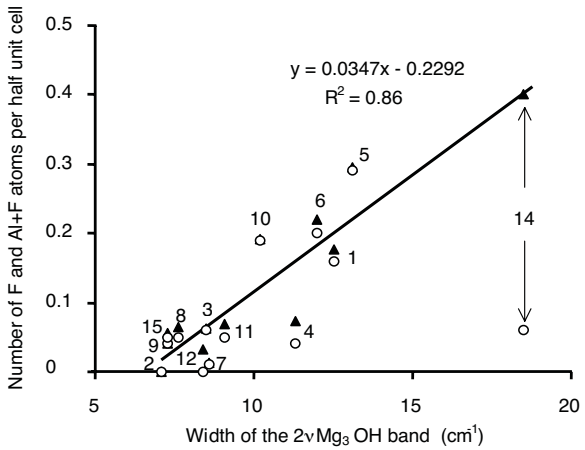

FIGURE 4. Width at half height of the $2\nu Mg_3OH$ band vs. number of F (circles) and Al + F (triangles) atoms per half unit cell (from Table 2): Numbers correspond to samples listed in Table 2.

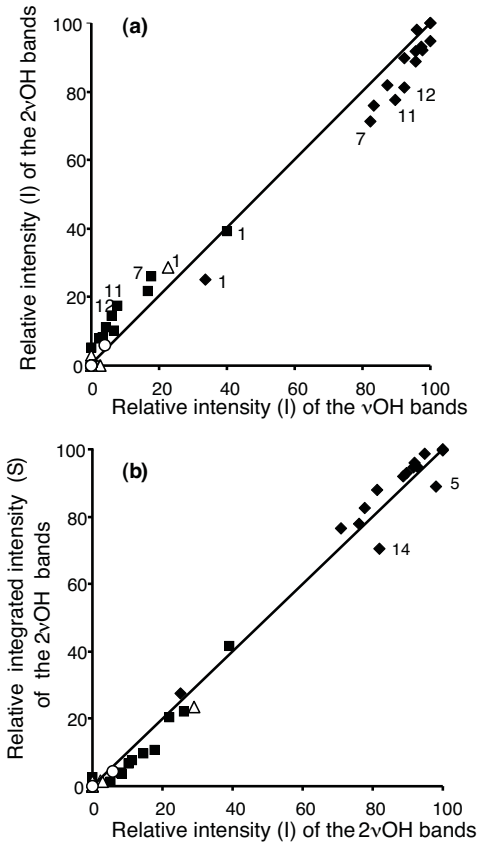

FIGURE 5. (**a**) Relative intensities (%) of both the νOH and 2νOH bands for the same OH groups, measured in the MIR and NIR regions, respectively; (**b**). Relative intensities vs. relative integrated intensities of the 2νOH bands for the same OH groupings in percentages. diamonds = Mg_3OH, squares = Mg_2FeOH, triangles = $MgFe_2OH$, circles = Fe_3OH. The 1:1 lines correspond to equal values from both methods. Numbers correspond to samples listed in Table 2.

ments. This overestimation can be explained by the presence of bandwidths with low intensity but relatively broad, and for this reason, the spectral decomposition provides better data for quantitative evaluation of the spectra.

The S of each band is determined by the number of absorbing centers of each type and by its absorption coefficient. In regard to quantitative results obtained previously from various clay minerals, the absorption coefficients of OH-vibration bands are assumed to be constant whatever the local chemistry around the OH groups (e.g., Slonimskaya et al. 1986; Besson and Drits 1997; Madejová et al. 1994). This assumption was used by these authors as a basis for the determination of the octahedral cation contents. As each OH group is bonded to 3 octahedral cations, 100% of the integrated intensities implies 300% of the composition of octahedral cations, and whatever the kind of octahedral cationic distribution:

$$\Sigma S(2\nu OH) = 100 \text{ and } \Sigma N_R = 3 \quad (1)$$

where N_R is the number of octahedral cations R per half unit cell in talc (Note that N_{Fe2+} is the number of octahedral Fe^{2+} + Ni, see above). The abundance of each octahedral cation is equal to the sum of the contribution of the cations to the S of the bands determined by those OH groups that contain the given cation in their nearest environment, and thus:

$$N_{Mg} = [3*S(2\nu Mg_3OH) + 2*S(2\nu Mg_2FeOH) + S(2\nu MgFe_2OH) + 2S(2\nu Mg_2AlOH)]/100$$
$$N_{Fe2+} = [3*S(2\nu Fe_3OH) + 2*S(2\nu Fe_2MgOH) + S(2\nu FeMg_2OH)]/100 \quad (2)$$
$$N_{Al} = S(2\nu Mg_2AlOH)]/100.$$

For some samples, $S(2\nu Mg_3OH) + S(2\nu Mg_2FeOH) + S(2\nu MgFe_2OH) + S(2\nu Mg_3OH) + S(2\nu Mg_2AlOH)$ is a little less than 100 (and then $N_{Mg} + N_{Fe2+} + N_{VI_{Al}} < 3$) because some small unattributed 2νOH bands are present, either due to unidentified OH groupings of talc or unidentified impurities.

The number of octahedral cations calculated from the NIR data were compared with that obtained from the structural formulae based on chemical analyses and given in Table 2 (Fig. 6). The results obtained by the two independent methods are in relatively good agreement. However, some departures from the 1:1 line are observed. Concerning Mg, the higher discrepancies are observed for samples 1 and 5 (0.25 and 0.26 Mg per half unit cell from NIR data less than from chemical data, respectively). The analytical error from the chemical data is in the ±0.01 atom range and cannot be invoked to explain these discrepancies. For sample 5, the underestimation of Mg by NIR is clearly due to an impurity. Indeed, bands at about 3620 and 7067 cm^{-1}, which are not due to talc, are clearly seen in Figures 2 and 3, respectively. These bands are probably due to kaolinite, in agreement with XRD data, which revealed a 7 Å ancillary phase. Taking into account this kaolinite impurity for sample 5 by excluding the integrated intensity of the 7067 cm^{-1} band of the summation (Eq. 1), N_{Mg} becomes 3, and would be drawn nearer to the 1:1 line in Figure 6. For sample 1, and in a lesser manner for all the samples containing Fe, the Mg content is underestimated (and thus the Fe content is correspondingly overestimated) from NIR

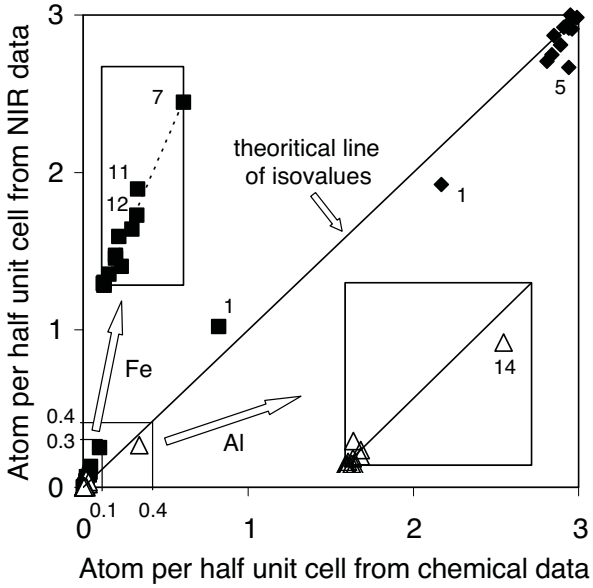

FIGURE 6. Number of atoms per half unit cell obtained through NIR measurement vs. that from chemical data given in Table 2. Diamonds = Mg, squares = Fe (+ Ni), triangles = Al. The left insert is a blow up of the Fe data (excluding sample 1).The dotted line is the correlation line obtained for Fe atom with the following equation y = 2.5814x – 0.0066 (R^2 = 0.97). The right insert is a blow up of the Al data. Numbers correspond to samples listed in Table 2.

data compared to the chemical analyses. No definite explanation can be given. Moreover, the number of Fe atoms given by chemical data is the maximum value because we assumed that all Fe was divalent and octahedral, although Mössbauer results showed that this was not actually the case (Table 2). No relation between Fe overestimation (or Mg underestimation) and F, which may link preferentially to certain cations groupings (Mg_3 here), is observed either. On the other hand, except for very Fe-rich sample 1, the data plot almost linearly (left insert in Fig. 6) with the following regression y = 2.5814x – 0.0066 (R^2 = 0.97), where x is the number of Fe atoms per half unit cell calculated from NIR data, and y is the number of Fe atoms per half unit cell given by the structural formulae deduced from chemical analyses (Table 2). Recalculating the data on the basis of an optimal octahedral occupancy ($N_{Mg} + N_{Fe2+} + N_{VI_{Al}} = 3$), leads to the equation y = 2.6192x - 0.003 (R^2 = 0.97), which does not change the trend significantly. Because the data for sample 1 do not suit the above equations (Fig. 6), the Fe overestimation (or Mg underestimation) from NIR cannot be explained by the different molar absorptions of the 2νOH bands. Problems in chemical measurements of small amounts of Fe or sample heterogeneity may also be invoked. For example, the number of Mg and Fe atoms represented in the literature for sample 1 [1.90 and 1.04, respectively (Robinson and Chamberlain 1984)] fits better with the NIR data. One must also keep in mind the fact that the NIR spectra were obtained by DRIFT and that diffuse reflectance is the radiation that penetrates into the sample and then emerges. DRIFT spectroscopy thus may be very sensitive to internal sample heterogeneity, at least in regard to the Fe con-

tent of talc. Because it was not possible to obtain good enough transmission spectra in the 2νOH region, the same quantitative approach as described above was performed in the νOH region (Fig. 2). The spectra of the Fe-rich samples (1, 7, 8, 11, and 12) were decomposed into their singular νOH bands to convert their S into octahedral cation abundances. Only the number of Fe and Mg atoms can be calculated, because uncertainty about the Al band was high. Comparison between these calculated values and the values obtained from chemical analyses is shown in Figure 7. Results from MIR data (transmission measurements) are in better agreement with data from chemical analyses than calculated data from NIR (diffuse reflectance measurements) (Fig. 6). As already noted by Lindberg and Snyder (1972), the two kinds of spectra may not necessarily be equivalent in a quantitative sense.

Concerning Al, the relatively good agreement between the number of cations calculated from the NIR data and these obtained from chemical analyses (right insert in Fig. 6) shows that our proposed assignment of the 7136 cm^{-1} band to $2\nu Mg_2AlOH$ is plausible. To our knowledge, this is the first time that this band has been reported in the literature for talc. On the other hand, for sample 14, because the chemical data indicates more Al than does NIR, which quantitatively measures ^{VI}Al only, the slight departure from the 1:1 line for this sample may be due to the presence of ^{IV}Al, which is in good agreement with RMN results (F. Martin, personal communication).

Cationic distribution

By an ordered cationic distribution is meant a tendency for certain groupings to occur more often than would be expected on the assumption of random mixing of octahedral cations. Actually, the measured relative integrated intensities (%S) of the observed bands have to be compared with the calculated values assuming a random distribution of octahedral cations, knowing their atomic proportions and the probabilities of occurrence of groupings as given in Table 4. The results of these calculations, using the atomic proportions of Mg, Fe, and Al measured from both chemical analyses and calculated NIR data, as explained above (Eq. 2), are given in Table 5. Several comments have to be made. Only 5 bands were observed compared to the 10 bands that have the probability of occurring. The bands that were never observed have a very low probability of occurring and, in most cases, are below the detection limits of NIR, which appears to be around 0.2–0.3 S% (Table 5). However, the $2\nu MgFeAlOH$ band for samples 1, 11, and 14, and the $2\nu MgAl_2OH$ band for sample 14, have not been observed but should occur above the detection limit. The overlapping of these bands with other major band may be invoked. However, for sample 14, which is very Al-rich, a preference for the Mg_2Al arrangement is not excluded.

TABLE 4. Probabilities of occurrence of OH band in case of a random distribution of 3 cations in the talc octahedral sheet, and assuming that the molar absorptions of the different OH groupings are identical

OH grouping	Probability
Mg_3OH	$[Mg]^3$
Mg_2FeOH	$3[Mg]^2[Fe]$
$MgFe_2OH$	$3[Mg][Fe]^2$
Fe_3OH	$[Fe]^3$
Mg_2AlOH	$3[Mg]^2[Al]$
$MgAl_2OH$	$3[Mg][Al]^2$
Fe_2AlOH	$3[Fe]^2[Al]$
$FeAl_2OH$	$3[Fe][Al]^2$
Al_3OH	$[Al]^3$
MgFeAlOH	6[Mg][Fe][Al]

Note: [R] = atomic proportion of the given octahedral cation.

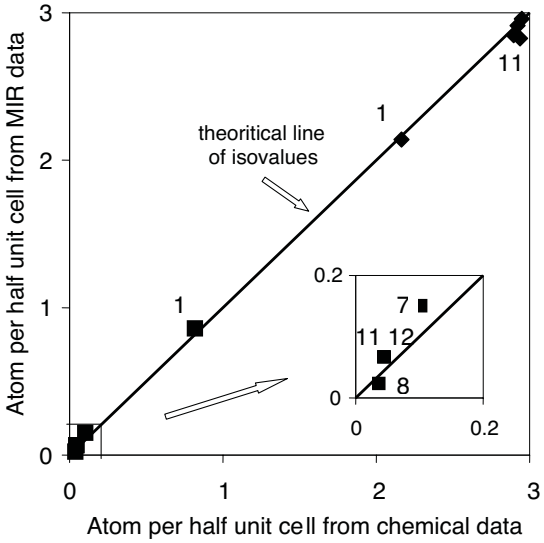

FIGURE 7. Number of atoms per half unit cell obtained through MIR measurement vs. that from structural formula given in Table 2. Diamonds = Mg, squares = Fe (+ Ni). Numbers correspond to samples listed in Table 2.

To interpret the Mg and Fe distribution in the studied talcs and to compare the data from individual samples more easily, the data from Table 5 were plotted in Figures 8a (atomic ratio from chemical analyses) and 8b (atomic ratio from NIR calculations). The lines are that of a random distribution of cations. Any departure from this line represents a deviation from the random distribution of both Fe and Mg octahedral cations.

When atomic proportions of Mg and Fe obtained by NIR are used (Fig. 8b), the data points fit the "random" line very well, meaning that the distribution of both Mg and Fe cations is random in all studied talcs. For sample 14, the departure of the $2\nu Mg_3OH$ to the random line is probably due to some ordering in distribution of Al within the octahedral sheet (see above). When atomic proportions of Mg and Fe obtained by chemical analyses are used (Fig. 8a), several departures from the "random" line are observed. Except for sample 1, the measured proportion of the Mg_2FeOH component is higher than expected, whereas the measured proportion of the Mg_3OH component is lower than expected. Because observed departures from the random line are those using chemical analyses, that result suggests that the departure from the "random" line is more probably due to defective analytical data (due to impurities and/or heterogeneity of samples) than to specific ordered distribution of Mg and Fe octahedral cations in the octahedral sheet of talc.

Proposal of structural formulae

To evaluate crystal chemistry of the studied talcs, their structural formulae were tentatively recalculated (Table 6) using chemical data obtained from NIR and Mössbauer data (Table 2). First, we used the number of octahedral cations (Mg, Fe, and

TABLE 5. Comparison between the 2νOH bands proportions (S%)

	$2\nu Mg_3OH$			$2\nu Mg_2FeOH$			$2\nu MgFe_2OH$			$2\nu Fe_3OH$			$2\nu Mg_2AlOH$			$2\nu MgAl_2OH$			$2\nu MgAlFeOH$			$2\nu Fe_2AlOH$			$2\nu FeAl_2OH$			$2\nu Al_3OH$		
No.	ob.	an.	NIR	ob.	an.	NIR	ob.	an.	NIR	ob.	an.	NIR	ob.	an.	NIR	ob.	an.	NIR	ob.	an.	NIR	ob.	an.	NIR	ob.	an.	NIR	ob.	an.	NIR
1	27.86	37.58	27.43	42.25	42.60	43.72	23.81	16.10	23.22	4.56	2.03	4.11	1.52	0.88	0.64	–	0.01	0.01	–	0.67	0.68	–	0.13	0.18	–	0	0	–	0	0
2	99.60	99.70	99.60	0.40	0.30	0.40	–	0	0	–	0	0	–	0	0	–	0	0	–	0	0	–	0	0	–	0	0	–	0	0
3	100	99.39	100	0	0.30	0	–	0	0	–	0	0	–	0.30	0	–	0	0	–	0	0	–	0	0	–	0	0	–	0	0
4	96.44	96.53	96.48	0.20	0.20	0.20	–	0	0	–	0	0	3.36	3.23	3.28	–	0.04	0.04	–	0	0	–	0	0	–	0	0	–	0	0
5	100	99.19	100	0	0.30	0	–	0	0	–	0	0	–	0.51	0	–	0	0	–	0	0	–	0	0	–	0	0	–	0	0
6	98.50	97.15	98.51	1.50	0.88	1.49	–	0	0.01	–	0	0	–	1.95	0	–	0.01	0	–	0.01	0	–	0	0	–	0	0	–	0	0
7	76.40	89.96	76.94	22.10	9.50	21.08	1.50	0.33	1.92	–	0	0.06	0	0.19	0	–	0	0	–	0.01	0	–	0	0	–	0	0	–	0	0
8	91.98	95.10	92.20	7.72	3.50	7.31	–	0.04	0.19	–	0	0	0.30	1.32	0.28	–	0.01	0	–	0.03	0.02	–	0	0	–	0	0	–	0	0
9	93.27	97.69	93.42	6.73	2.09	6.43	–	0.01	0.15	–	0	0	–	0.20	0	–	0	0	–	0	0	–	0	0	–	0	0	–	0	0
10	95.90	98.09	95.96	4.10	1.70	3.99	–	0.01	0.06	–	0	0	–	0.20	0	–	0	0	–	0	0	–	0	0	–	0	0	–	0	0
11	82.77	93.83	82.58	10.62	4.29	11.64	1.30	0.07	0.55	–	0	0.01	5.31	1.75	4.67	–	0.01	0.09	–	0.05	0.44	–	0	0.01	–	0	0	–	0	0
12	88.34	92.41	88.79	9.65	4.18	8.91	–	0.06	0.30	–	0	0	2.01	3.21	1.86	–	0.04	0.01	–	0.10	0.12	–	0	0	–	0	0	–	0	0
13	78.00	/	78.21	20.40	/	20.03	1.60	/	1.71	–	/	0.05	–	/	0	–	/	0	–	/	0	–	/	0	–	/	0	–	/	0
14	70.50	69.39	73.31	2.60	1.78	2.11	–	0.02	0.02	–	0	0	26.90	25.19	21.87	–	3.05	2.17	–	0.43	0.42	–	0	0	–	0.03	0.02	–	0.12	0.07
15	95.55	97.67	95.62	3.74	1.71	3.63	–	0.01	0.05	–	0	0	0.71	0.60	0.69	–	0	0	–	0.01	0.02	–	0	0	–	0	0	–	0	0

Notes: ob. = obtained by spectral decomposition; an. = calculated assuming a random distribution of octahedral cations measured from chemical analyses; NIR = calculated assuming a random distribution of octahedral cations measured from NIR; # =sample; – = not observed; / = not measured.

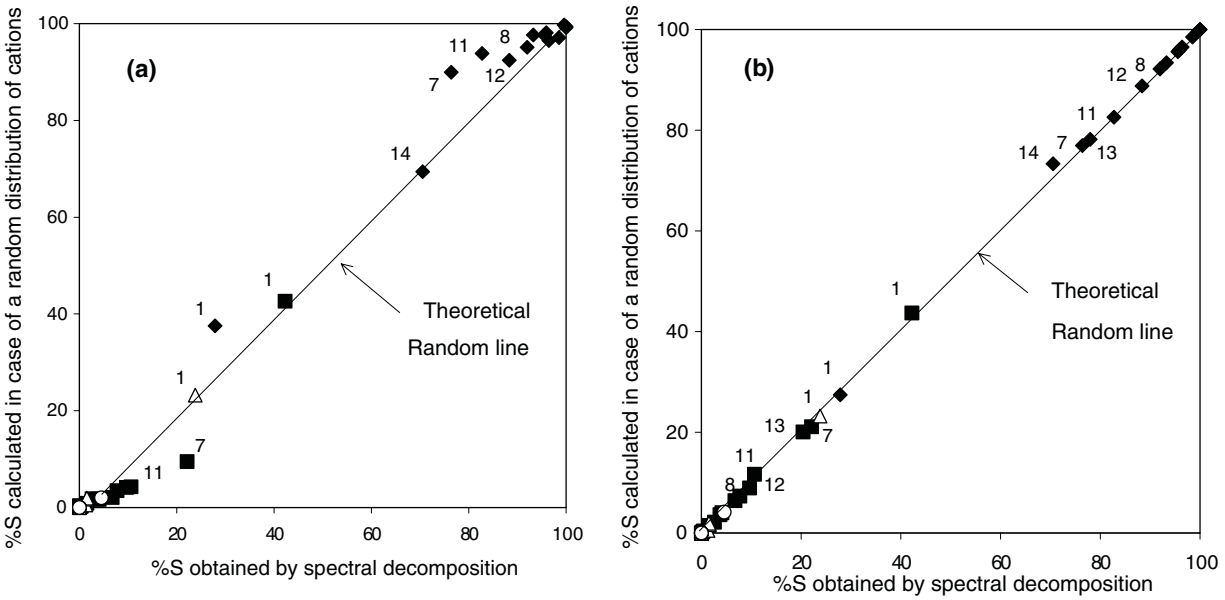

FIGURE 8. Measured relative integrated intensities (%S) of the observed bands obtained by spectral decomposition vs. the values calculated assuming a random distribution between octahedral cations (Table 5) using atomic ratio from: (**a**) chemical analyses (Table 2) (**b**) calculated NIR data (Fig. 6). Diamonds = $2\nu Mg_3OH$; squares = $2\nu Mg_2FeOH$; triangles = $MgFe_2OH$, circles = Fe_3OH. Data points would plot on the "theoretical random line" if cations are randomly distributed. Numbers correspond to samples listed in Table 2.

Al) as calculated above from S of 2νOH bands (Eq. 2). Second, assuming that Fe calculated from NIR data was strictly Fe^{2+} (because only Fe^{2+} is measured trough identified OH groupings), we calculated atomic amounts of Fe^{3+} in tetrahedral and octahedral coordination from Mössbauer data (Table 2). Third, we assumed that the difference between regression line and octahedral Al content found from NIR data (right insert in Fig. 6) corresponds to the tetrahedral Al content. Fourth, we tentatively calculated the F content using the regression equation $y = 0.0347x - 0.2292$ where y is the number of Al + F atoms per half unit cell, and x the width of the $2\nu Mg_3OH$ band (Fig. 4), using the width of the $2\nu Mg_3OH$ band and the Al content found from NIR data.

For samples 1, 7, 8, 10, 12, and 14, a slight excess in the octahedral occupancy is observed. Taking into account the relatively low precision of the Mössbauer measurements due to the low Fe contents of the sample together with the failure to identify OH groupings involving Fe^{3+}, the amounts of Fe^{3+} are only indicative. Note that for sample 1, the amount of Fe^{2+} is actually the amount of Fe^{2+} + Ni, as explained above. In fact, the presence of Ni would decrease the calculated amount of Fe^{3+}, although not enough to account for the relatively high excess octahedral occupancy (the number of Ni atoms would be near 0.5 to obtain an octahedral occupancy of 3). For samples 2, 3, 5, and 6, the structural formulae are good. Note that samples 3 and 5 are pure Mg talcs. For sample 13, the lack of Mössbauer data does not permit to classify it in the category where octahedral occupancy is 3. For samples 4, 9, 11, and 15, the occurrence of vacancies is indicated. Vacancies may be explained in part by the trivalent cations in some dioctahedral OH groupings such as $Fe^{3+}Mg\square OH$ and $AlMg\square OH$ (where □ is a vacant site), to balance the charge due to heterovalent substitutions. For sample 4, the deficient octahedral occupancy is mainly due to unattributed bands that are probably due to impurities. These impurities are possibly responsible for the out-of-trend large width of the $2\nu Mg_3OH$ band (Fig. 4). For this sample, the actual F content of the talc given in Table 6 is then clearly overestimated. A more

TABLE 6. Structural formulae of talcs as calculated from NIR and Mössbauer data

	1	2	3	4	5	6	7	8	9	10	11	12	13	14	15
Si	3.999	4	4	4	4	3.990	3.844	3.984	3.992	3.991	3.963	3.975	4	3.925	3.989
^{IV}Al	0	0	0	0	0	0	0	0	0	0	0	0	0	0.071	0
^{IV}Fe^{3+}*	0.001	–	–	–	–	0.010	0.156	0.016	0.008	0.009	0.037	0.025		0.004	0.011
	±0.001					±0.002	±0.005	±0.002	±0.001	±0.002	±0.003	±0.005	–	±0.001	±0.002
Mg	1.924	2.996	3	2.911	3	2.985	2.749	2.914	2.918	2.959	2.809	2.869	2.764	2.705	2.923
Fe^{2+}	1.022	0.004	0	0.002	0	0.015	0.251	0.077	0.067	0.041	0.132	0.096	0.236	0.026	0.037
^{VI}Fe^{3+}*	0.078	–	–	–	–	0	0.066	0.020	0.004	0.013	0	0.046	–	0.013	0.009
	±0.017						±0.012	±0.005	±0.001	±0.003		±0.002		±0.003	±0.002
^{VI}Al	0.015	0	0	0.033	0	0	0	0.003	0	0	0.05	0.02	0	0.269	0.007
Σ oct.	3.039	3.000	3.000	2.946	3.000	3.000	3.066	3.014	2.989	3.013	2.991	3.031	3.000	3.013	2.976
F	0.19	0.02	0.07	0.13	0.23	0.19	0.07	0.03	0.02	0.13	0.04	0.04	0.03	0.07	0.02

Note: – = no Mössbauer data.
*The precision of measurement is issued from Mössbauer decomposition software.

realistic value for the F content may be obtained by projection on to the regression line (Fig. 4), which gives 0.04 atoms of F per half unit cell—a value that appears very well with the measured chemical data (Table 2). For all the other samples, the contents of F obtained as described above are realistic in regard to the measured chemical data (Table 2).

ACKNOWLEDGMENTS

We are grateful to E. Ferrage for helpful discussions and J. Ferret and R. Baëza (Talc de Luzenac Europe) for their financial support.

REFERENCES CITED

Alper, N.L., Keiser, W.E., and Szymanski, H.A. (1964) IR—Theory and practice of infrared spectroscopy, p. 380. New York, Plenum Press.

Besson, G. and Drits, V.A. (1997) Refined relationships between chemical composition of dioctahedral fine-dispered mica minerals and their infrared spectra in the OH stretching region. Part I: Identification of the stretching band. Clays and Clay Minerals, 45, 158–169.

Farmer, V.C. (1974) The layer silicates. In V.C. Farmer, Ed., The infrared Spectra of Minerals, 331–364. Mineralogical Society, London.

Ferrage, E., Martin, F., Boudet, A., Petit, S., Fourty, F., Jouffret, F., Micoud, P., de Parseval, Ph., Salvi, S., Bourgerette, C., Ferret, J., Saint-Gérard, Y., Buratto, S., and Fortuné, J.P. (2002) Talc as nucleating agent of polypropylene: morphology induced by lamellar particles addition and interface mineral-matrix modelization. Journal of Material Science, 37, 1561–1573.

Galan-Huertos, E. and Rodas, M. (1973) Contribución al estudio mineralógico de los depósitos de Talco de Puebla de Lillo (León, España). Boletin Geológico y Minero, 84, 347–365.

Gonzalez, A., de Saja, J.A., and Alonso, J. (1995) Morphology and tensile properties of compression-moulded talc-filled polypropylene. Materials, Plastics, Rubber & Composites Processing and Applications, 24, 131.

Hawthorne, F.C. and Waychunas, G.A. (1988) Spectrum-fitting methods. In Reviews in Mineralogy: Spectroscopic methods in mineralogy and geology, 18, 63–98. Mineralogical Society of America, Washington, D.C.

Kulke, H. and Schreyer, W. (1973) Kyanite-talc schist from Sar a Sang, Afghanistan. Earth and Planetary Science Letters, 18, 324–328.

Lindberg, J.D. and Snyder, D.G. (1972) Diffuse reflectance spectra of several clay minerals. American Mineralogist, 57, 485–493.

Madejová, J., Komadel, P., and Cicel, B. (1994) Infrared study of octahedral site populations in smectites. Clay Minerals, 29, 319–326.

Madejová, J., Bujdák, J., Petit, S., and Komadel, P. (2000) Effects of chemical composition and temperature of heating on the infrared spectra of Li-saturated dioctahedral smectites. Part (II) Near-infrared region. Clay Minerals, 35, 753–761.

Martin, F., Micoud, P., Delmotte, L., Maréchal, C., Le Dred, R., de Parseval, Ph., Mari, A., Fortuné, J.P., Salvi, S., Béziat, D., Grauby, O., and Ferret, J. (1999) The structural formula of talc from the Trimouns deposit, Pyrénées, France. Canadian Mineralogist, 37, 4, 975–984.

Menczel, J. and Varga, J. (1983) Influence of nucleating agents on crystallization of polypropylene. I. Talc as nucleating agent. Journal of Thermal analysis, 28, 161–174.

Moine, B., Fortune, J.P., Moreau, P., and Viguier, F. (1989) Comparative Mineralogy, Geochemistry, and Conditions of Formation of Two Metasomatic Talc and Chlorite Deposits: Trimouns (Pyrenees, France) and Rabenwald (Eastern Alps, Austria). Economic Geology, 84, 1398–1416.

Petit, S., Madejová, J., Decarreau, A., and Martin, F. (1999) Characterization of octahedral substitutions in kaolinites using near infrared spectroscopy. Clays and Clay Minerals, 47, 103–108.

Rancourt, D.G., McDonald, A.M., Lalonde, A.E., and Ping, J.Y. (1993) Mössbauer absorber thicknesses for accurate site populations in Fe-bearing minerals. American Mineralogist, 78, 1–7.

Robert, J.-L. and Kodama, H. (1988) Generalization of the correlations between hydroxyl-stretching wavenumbers and composition of micas in the system K_2O-MgO-Al_2O_3-SiO_2-H_2O: a single model for trioctahedral and dioctahedral micas. American Journal of Science, Wones Volume, 288-A, 196–212.

Robert, J.-L., Della Ventura, G., Welch, M., and Hawthorne, F.C. (2000) The OH-F substitution in synthetic pargasite at 1.5 kbar, 850°C. American Mineralogist, 85, 926–931.

Robinson, G.W. and Chamberlain, S.C. (1984) Famous mineral localities: the Sterling Mine Antwerp, New York. The Mineralogical Record, July-August, 199–216.

Rywak, A.A. and Burtlich, J.M. (1996) The crystal chemistry and thermal stability of sol-gel prepared fluorine-substituted talc. Physic and Chemistry of Minerals, 23, 418–431.

Schandl, E.S., Sharara, N.A., and Gorton, M..P. (1999) The origin of the Atshan talc deposit in the Hamata area, Eastern Desert, Egypt: A geochemical and mineralogical study. Canadian Mineralogist, 37, 1211–1227.

Schärer, U., de Parseval, Ph., Polvé, M., and de Saint Blanquat, M. (1999) Formation of the Trimouns talc-chlorite deposit (Pyrenees) from persistent hydrothermal activity between 112 and 97 Ma. Terra Nova, 11, 30–37.

Slonimskaya, M.V., Besson, G., Dainyak, L.G., Tchoubar, C., and Drits, V.A. (1986) Interpretation of the IR spectra of celadonites and glauconites in the region of OH-stretching frequencies. Clay Minerals, 21, 377–388.

Tiganis, B.E., Shanks, R.A., and Long, Y. (1996) Effects of Processing on the Microstructure, Melting Behavior and Equilibrium Melting Temperature of Polypropylene. Journal of Applied Polymer Science, 59, 663–671.

Tornos, F. and Spiro, B.F. (2000) The geology and isotope geochemistry of the talc deposits of Puebla de Lillo (Cantabrian zone, northern Spain). Economic Geology, 95, 1277–1296.

Wilkins, R.W.T. and Ito, J. (1967) Infrared spectra of some synthetic talcs. American Mineralogist, 52, 1649–1661.

MANUSCRIPT RECEIVED FEBRUARY 24, 2003
MANUSCRIPT ACCEPTED AUGUST 19, 2003
MANUSCRIPT HANDLED BY SIMONA QUARTIERI